PCCP

PAPER

View Article Online
View Journal | View Issue

Cite this: *Phys. Chem. Chem. Phys.*, 2015, **17**, 19315

Effects of stereoelectronic interactions on the relativistic spin–orbit and paramagnetic components of the ^{13}C NMR shielding tensors of dihaloethenes†

Renan V. Viesser,[a] Lucas C. Ducati,[b] Jochen Autschbach[c] and Cláudio F. Tormena*[a]

Received 7th April 2015,
Accepted 26th June 2015

DOI: 10.1039/c5cp02026c

www.rsc.org/pccp

In this study, stereoelectronic interactions were considered to explain the experimental difference in the magnitude of the known heavy-atom effect on the ^{13}C NMR chemical shifts in *cis*- and *trans*-1,2-dihaloethene isomers (halo = F, Cl, Br or I). The experimental values were compared to the calculated values with various DFT functionals using both the nonrelativistic approach (NR) and the relativistic approximations SR-ZORA (SR) and SO-ZORA (SO). NBO and NLMO contributions to the ^{13}C NMR shielding tensors were determined to assess which stereoelectronic interactions have a more important effect on the shielding tensor in each principal axis system (PAS) coordinate. These analyses associated with the orbital rotation model and the HOMO–LUMO energy gap enable rationalization of trends between *cis* and *trans* isomers from fluorine to iodine derivatives. Both paramagnetic and SO shielding terms were responsible for the observed trends. It was possible to conclude that the steric interactions between the two iodine atoms and the hyperconjugative interactions involving the halogen lone pairs (LP(X)) and $\pi_{C=C}$*, $\sigma_{C=C}$* and σ_{C-X}* antibonding orbitals are responsible for the lower ^{13}C NMR shielding for the *cis* isomers of the bromine and the iodine compounds than that of the *trans* isomers.

1. Introduction

Relativistic effects in NMR parameters have interested scientists because of the strong influence of such effects on molecules containing heavy atoms (HAs).[1–6] In the last three decades, many theoretical studies have reported these effects on chemical shifts, nuclear shielding tensors and indirect spin–spin coupling constants using various electronic structure methods and relativistic approaches.[7–18]

Two common types of relativistic effects known for the shielding constants (σ) are the heavy-atom effect on its own shielding (HAHA) and the heavy-atom effect on the shielding of a nearby light atom (LA), such as carbon or hydrogen (HALA).[1,19] It has been reported[20,21] for the HX (X = F, Cl, Br, I or At) and H_2X (X = O, S, Se, Te or Po) systems, that spin–orbit–HALA effect on the ^{1}H NMR chemical shifts are very important. A decrease in the chemical shift of the nucleus bound directly to the halogen substituent is frequently observed, especially for bromine and iodine compounds; this effect is called the normal halogen dependence (NHD).[22–24]

The spin–orbit (SO) term for the nuclear shielding tensor is recognized to be primarily responsible for the relativistic effects on the chemical shift of a light nucleus in HALA systems. This phenomenon has been understood as the interaction between the SO coupling of the HA and the spin-dependent Fermi contact (FC) and spin-dipolar (SD) mechanisms.[25] The induced spin polarization can be transmitted through a covalent bond from a HA to a neighboring LA nucleus, resembling the mechanism for the transmission of the FC term in indirect spin–spin coupling constants (FC/FC mechanism).[1,25,26] The SO/FC is usually reported as the most important mechanism that explains the HA effect on the ^{13}C NMR chemical shift, whereas the SO/SD transmission mechanism is considered to be small. However, in the case of iodine compounds, these mechanisms can be modified by the presence of lone pairs on a nearby iodine atom.[25] Further details are discussed below.

Many factors can influence the intensity of SO for the shielding tensor (σ_{SO}), mainly due to the similarity between the SO/FC and FC/FC transmission mechanics. As the first factor, the σ_{SO} can be associated with the s-character of the

[a] *Chemical Institute, University of Campinas – UNICAMP, P.O. Box 6154, 13083-970 Campinas, SP, Brazil. E-mail: tormena@iqm.unicamp.br*
[b] *Institute of Chemistry, University of São Paulo, CP 26077, 05513-970 São Paulo, SP, Brazil*
[c] *Department of Chemistry, University at Buffalo, State University of New York, Buffalo, New York 14260-3000, USA*

† Electronic supplementary information (ESI) available. See DOI: 10.1039/c5cp02026c

valence orbitals of the LA in the HA–LA bond. Kaupp *et al.*[25] observed this behavior based on the increase of the ^{13}C NMR shielding tensor from iodoethane (s% lower) to iodoacetylene (s% higher). The same authors[25] and Hyvärinen *et al.*[26] also show that the σ_{SO} has an angular dependence of three bonds, associated with the known Karplus relationship. These factors are generally connected with better FC transmission and high spin density of the LA nucleus, which has been related to the s-character of HA–LA bond.

The SO/FC transmission mechanism must depend significantly on the overlap and the energy gaps between the bonding and the antibonding orbitals, in which some studies[25–29] have found an inverse relationship among the energy gaps and σ_{SO}. Taking these considerations into account, any stereoelectronic interaction that increases a relevant energy gap between the ground and the excited states has the potential to decrease the corresponding SO contribution of the SO/FC and SO/SD cross terms. Recently, our group[29] observed that hyperconjugative interactions involving the σ_{C-X}^{*} orbital (X = Cl, Br, I) can affect the SO term and the intensity of the HALA effect on the ^{13}C NMR chemical shift in halocyclohexane and halopyran derivatives.

Recently, some transition-metal complexes studies, especially the work of Vícha *et al.*,[30] have demonstrated the role of the d-character of the metal–ligand bond on the SO magnitude linking NMR and EPR data, such as σ_{SO}, the *g*-tensor and the *A*-tensor. These authors demonstrated that the d-character of occupied and virtual MOs was connected with the σ_{SO} in iridium compounds, whereas the s-character and energy gap did not show significant correlations with experimental trends.

Other individual effects on the NMR shielding observed in theoretical studies[9,31] are also interesting, such as the exchange–correlation (XC) potential and the effects of dispersion, particularly if the calculations are performed with DFT methods. The exchange–correlation potential is more important than the dispersion in geometry optimizations, showing corrections of $\sim$5 ppm for ^{13}C NMR shielding constants, whereas the value of the dispersion correction is usually very small ($<$0.5 ppm).[9]

An interesting aspect is that the nuclear shielding depends not only on the chemical structure but also on the molecular orientation within the external magnetic field B_0. The shielding tensor σ can be written in terms of a molecule-fixed principal axis system (PAS) and the principal components σ_{11}, σ_{22} and σ_{33} of the shielding. In the PAS representation, the isotropic shielding is the average of the principal components.[32,33]

There are several quantum chemistry packages available for relativistic calculations of σ_{SO}. For example, the Amsterdam density functional (ADF)[34] package utilizes the ZORA (zeroth-order regular approximation) Hamiltonian. ZORA is an approximate two-component relativistic method that has been shown to deliver quite accurate chemical shifts and NMR *J*-couplings[21] for heavy element systems. The use of a fully relativistic Hamiltonian or other approximate two-component methods[35–39] is also possible. This work is based on ZORA calculations because of the availability of analysis tools for the shielding tensor obtained from relativistic calculations. The ZORA magnetic property expressions are very similar to the well-known nonrelativistic Ramsey equations, which facilitates the interpretation of the results in commonly known terms. The total shielding can – as in the nonrelativistic limit – be written as a sum of a diamagnetic component (σ_{dia}) and a paramagnetic component (σ_{para}). These components include scalar relativistic effects. In addition, there is a SO coupling contribution (σ_{SO}). In two-component relativistic calculations, the magnetic nuclear shielding tensor for the ground state can be written formally as[16]

$$\sigma_{u,v} = \langle\psi_0|\mathrm{DS}|\psi_0\rangle + 2\,\mathrm{Re}\sum_{j\neq 0}\frac{\left\langle\psi_0|(\mathrm{OP}+\mathrm{FC}+\mathrm{SD})|\psi_j\right\rangle\left\langle\psi_j|(\mathrm{OZ}+\mathrm{SZ})|\psi_0\right\rangle}{E_0-E_j}; \quad (1)$$

Eqn (1) represents one of the tensor elements ($u, v = x, y, z$); ψ_0, E_0 and ψ_j, E_j are the wavefunctions and energies for the ground state and excited state, respectively. The operators are the relativistic analogs of the diamagnetic shielding (DS), orbital paramagnetic (OP), orbital Zeeman (OZ), spin-Zeeman (SZ), FC and SD operators. In the two-component ZORA framework, these operators can be written in a similar way to the nonrelativistic ones.[40] FC, SD and SZ are electron-spin dependent, whereas OP, OZ and DS are not. In the absence of SO coupling, FC, SD and SZ do not contribute to the shielding. The usual paramagnetic component of the shielding tensor is then given by the OP–OZ operator combination. SO effects can arise in the OP–OZ mechanism *via* the wavefunctions/orbitals, but the majority of SO effects are typically revealed in the OP–SZ and in particular in the (FC + SD)−(OZ + SZ) cross terms. At the SO level, there is no clear distinction between paramagnetic and SO effects in the sense that they both contribute in the sum-over-states part of eqn (1). The analysis connects most straightforwardly with the scalar relativistic (SR) or nonrelativistic levels if 'paramagnetic' is identified with the OP–OZ mechanism, keeping in mind that the numerical results for this mechanism may differ somewhat between SR and SO calculations. Both paramagnetic and SO contributions are dependent on the energy difference between the ground and excited states according to the denominator of eqn (1).[16]

The calculations for this work employed linear-response DFT. The paramagnetic and SO shielding contributions (second term of eqn (1)) may be written in terms of Kohn–Sham (KS) MOs as[41]

$$\sigma_{u,v} = \mathrm{const.}\,\mathrm{Re}\sum_{i}^{\mathrm{occ}}\sum_{a}^{\mathrm{unocc}}\frac{\langle\varphi_i|\mathrm{H}_u^B|\varphi_a\rangle\langle\varphi_a|\mathrm{H}_v^\mu|\varphi_i\rangle}{\varepsilon_i-\varepsilon_a}; \quad (2)$$

Eqn (2) is associated with the orbitals and orbital energies φ_i, ε_i and φ_a, ε_a for occupied and unoccupied canonical KS MOs, respectively. The superscripts of the NMR perturbation operators H_u^B and H_v^μ refer to the magnetic field (B), *i.e.*, OZ and SZ, and the nuclear spin magnetic moment (μ), *i.e.*, OP, FC, and SD. They are described in detail in ref. 41. Note that H_u^B formally also includes the response of the KS potential to the magnetic-field perturbation. For a KS potential that depends on only the electron density, this contribution vanishes because the magnetic field

does not perturb the density but only the orbital current–density and – in SO calculations – the spin density.

Although the effect of HA on the ^{13}C chemical shift is known, for example, in iodine compounds, there are some experimental data that are not completely understood. As an example, consider the experimental variations in the ^{13}C NMR chemical shifts among the *cis* and *trans* isomers of the 1,2-dihaloethenes, mainly between the iodine derivatives, for which the difference in the ^{13}C chemical shift is approximately 17 ppm between the *cis* and *trans* isomers (*trans* more shielded).[42–44]

To investigate why this difference occurs between *cis* and *trans* isomers, the theoretical and experimental data for the *cis* and *trans* isomers of 1,2-dihaloethenes (halo = F, Cl, Br or I) were evaluated. In this study, it is demonstrated how the stereoelectronic interactions can influence the σ_{para} and σ_{SO} components of the nuclear shielding tensor and, therefore, the intensity of the HA effect on ^{13}C NMR chemical shifts for the *cis* and *trans* isomers of 1,2-diiodoethenes. The role of stereoelectronic interactions in the σ_{para} and σ_{SO} components has been rationalized on the basis of the combination of shielding tensor components, the coordinates of the PAS and localized orbitals analysis. These analogies allowed us to understand how the localized orbitals contributions for the ^{13}C NMR shielding in each PAS coordinate for the studied systems.

2. Experimental and computational details

2.1 NMR measurements

The chlorine and bromine compounds were commercially available, and the iodine isomers were synthesized according to a procedure described in the literature.[45] The 1,2-difluoroethene isomers were not experimentally studied because they are gaseous compounds. The experimental ^{13}C NMR chemical shifts for the fluorine derivatives were obtained from the literature.[46]

The ^{13}C NMR spectra were recorded on a Bruker Avance III 600 spectrometer operating at 600.17 MHz and 150.92 MHz for ^{1}H and ^{13}C, respectively. The samples were prepared as solutions of 15 mg of the solute in 0.7 ml of $CDCl_3$ or DMSO-d_6.

2.2 Computational details

All of the calculations for the geometry optimization, the NMR shielding and the NBO were performed with four different DFT functionals (B3LYP,[47] PBE0,[48] KT2[49] and BP86[50]), using a triple-ζ doubly polarized Slater-type basis set (TZ2P) within the Amsterdam density functional (ADF2013) software package.[51]

Optimized geometries for the *cis*- and *trans*-1,2-dihaloethene (halo = F, Cl, Br or I) compounds were obtained using the nonrelativistic and with the relativistic scalar ZORA (SR-ZORA) approaches. ^{13}C NMR shielding tensors were calculated using the nonrelativistic (NR) approach and the two-component relativistic methods: the scalar ZORA (SR) and the spin–orbit ZORA (SO).[52,53] For all systems studied in this work, the gauge origin was placed at the carbon atom.

The diamagnetic and SO components of the shielding tensors were obtained from the SO calculations, whereas the paramagnetic component was estimated from the SR. In the results, the SO contributions to the diamagnetic shielding were negligible.

The ^{13}C NMR chemical shifts were obtained using the nuclear shielding tensor calculated for the TMS reference. The chemical shifts (δ_i) were calculated using the equation below, where δ_i is the carbon shielding tensor of the dihaloethenes, and δ_{ref} is the carbon shielding tensor for the TMS.

$$\delta_i = \sigma_{ref} - \sigma_i \quad (3)$$

Geometry and NMR shielding calculations were also performed to evaluate the accuracy of the TZ2P and QZ4P basis set and the solvent effect (chloroform), using the conductor-like screening model for realistic solvent (COSMO-RS).[54,55] Geometry optimizations and SCF calculations were performed using numerical integration 6.0 based on the Voronoi quadrature scheme.

Orbital analysis was evaluated using the natural bond orbital (NBO 6.0 code)[56] analysis, as implemented in the ADF program, which was used to generate the scalar relativistic NBOs and NLMOs at the KT2 level of theory. The graphical representations of the shielding tensors were generated as in previous works by Zurek *et al.*[57] and Autschbach.[58] The NBO and NLMO contributions for the principal components of the shielding tensor (σ_{11}, σ_{22} and σ_{33}) were determined according to references[41,59] and further rationalized with the help of orbital rotation models.[60,61]

3. Results and discussion

3.1 Experimental δ ^{13}C NMR results

Table 1 reports the experimental results of the ^{13}C NMR chemical shifts for the *cis*- and *trans*-1,2-dihaloethenes (halo = Cl, Br or I) in a non-polar solvent ($CDCl_3$) and in a polar solvent (DMSO-d_6). The experimental values of the ^{13}C NMR chemical shifts for the *cis* and the *trans* isomers of chlorine and bromine derivatives did not exhibit significant variations ($\sim$1.0 ppm) in non-polar and in polar solvents, which might be due to the low flexibility of the π system.

It can be observed from Table 1 that the ^{13}C chemical shift for the *trans* isomer is more shielded (lower frequency) than for the *cis* isomer, especially for iodine; however, the reason for this experimental behavior is not yet clear, and the present study intents to shed light on the question.

Table 1 Experimental ^{13}C NMR chemical shifts (ppm) obtained for *cis*- and *trans*-1,2-dihaloethenes in $CDCl_3$ and DMSO-d_6

Isomer	Solvent	Cl	Br	I
cis	$CDCl_3$	120.8	113.6	97.8
	DMSO-d_6	121.1	114.6	—
trans	$CDCl_3$	120.3	107.3	80.4
	DMSO-d_6	120.4	108.2	—

3.2 Choice of the DFT functional and ZORA hamiltonian

To gain insight regarding the origin of the difference in Table 1, it was necessary to obtain theoretical values in reasonable agreement with experimental values. To this end, four different DFT functionals were applied to calculate the δ ^{13}C NMR.

Fig. 1 compares the experimental and the theoretical δ ^{13}C NMR for *cis*- and *trans*-1,2-dihaloethenes, for which the theoretical values for the halogen series were calculated by the KT2 and BP86 pure GGA functionals and the B3LYP and PBE0 hybrid functionals. It is observed (Fig. 1) that the KT2 level of theory gives the best agreement with the experimental values, with deviations smaller than 6 ppm for both isomers, though accuracy was better for the *trans* isomer.

Fig. 1 also shows that the HA leads to shielding for nearby ^{13}C, which is more pronounced in the *trans* isomer, in agreement with the experimental results, in which the differences in the chemical shift among the isomers of the diiodoethene are approximately 17 ppm (Table 1).

Relativistic corrections are well suited to evaluating the HA effect and the decay trend of the chemical shifts in halogenated series, as observed in Fig. 2. For the fluorine and chlorine compounds, the SO relativistic corrections were not important because of the small nuclear charges of the halogen.

However, the bromine and the iodine compounds displayed (Fig. 2) a strong influence of relativity and spin-dependent terms; thus, the SO-ZORA approximation showed an adequate correlation with the experimental results. If only the scalar relativistic (SR-ZORA) or the nonrelativistic (NR) approximation was included, the deviations from the experimental ^{13}C NMR chemical shifts would increase by approximately 30–35 ppm (Fig. 2).

3.3 Analysis of basis function and inclusion of the solvent model

The experimental and theoretical ^{13}C NMR chemical shifts were compared for the *cis* and *trans* isomers of diiodoethene using the KT2 method with two different basis sets, *i.e.*, TZ2P and QZ4P, and including or not including the solvent effect by means of the COSMO solvent model. The results are displayed in Fig. 3.

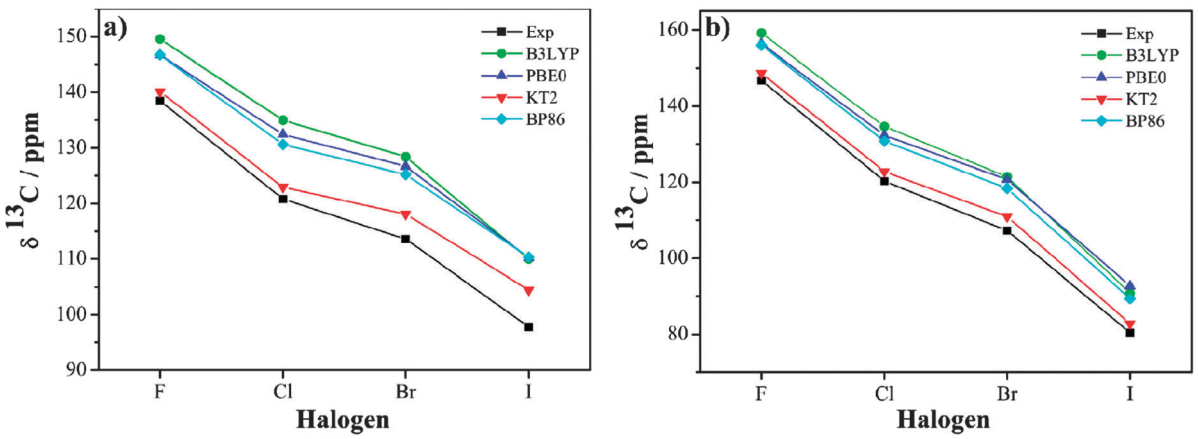

Fig. 1 Comparison between the experimental (Exp) and the theoretical ^{13}C NMR chemical shifts calculated using four different functionals (B3LYP, PBE0, KT2 and BP86) with the SO-ZORA Hamiltonian: (a) *cis*-1,2-dihaloethenes and (b) *trans*-1,2-dihaloethenes.

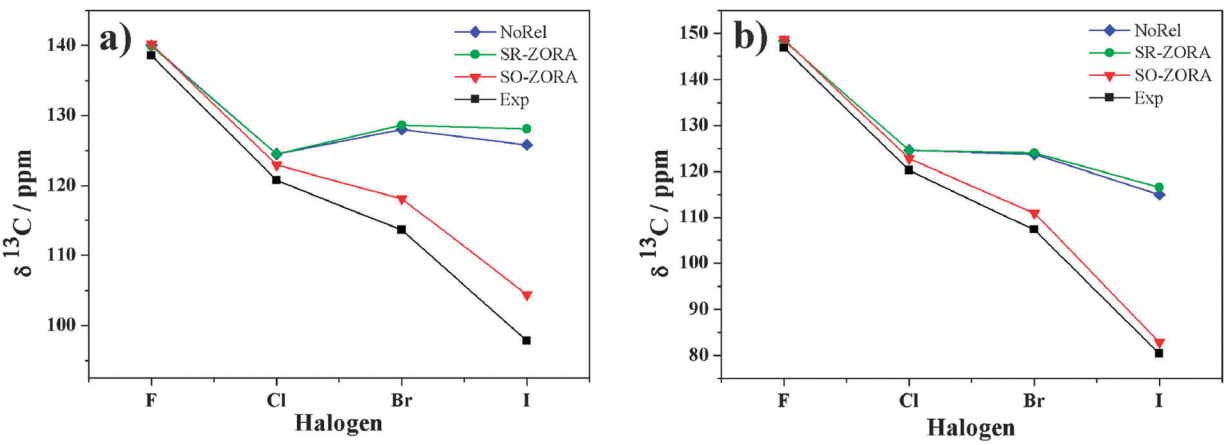

Fig. 2 Comparison between the experimental (Exp) and the theoretical ^{13}C NMR chemical shifts, calculated using the KT2/TZ2P functional with the non-relativistic (NR), the scalar ZORA (SR-ZORA) and the spin–orbit ZORA (SO-ZORA) Hamiltonians: (a) *cis*-1,2-dihaloethenes and (b) *trans*-1,2-dihaloethenes.

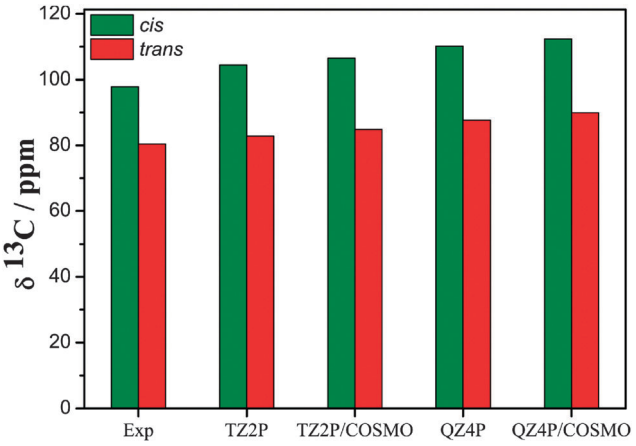

Fig. 3 The experimental (Exp) and the calculated ^{13}C NMR chemical shifts for *cis*- and *trans*-1,2-diiodoethene using the KT2/SO-ZORA level of theory with the TZ2P or the QZ4P basis set, with and without the COSMO-RS solvent model.

It is observed that the results nearest the experimental values were obtained using the smaller basis set TZ2P and when the solvent effect using the COSMO solvent model was not included. The deviations of the experimental values were 6.6 and 2.4 ppm for the *cis* and *trans* isomers, respectively. The deviations increased when the QZ4P basis set and the COSMO solvent model were applied, reaching values up to 14.5 and 9.6 ppm for the *cis* and the *trans* isomers, respectively. This result must be attributed to an error cancellation at the TZ2P/gas-phase level or poor performance of the COSMO model. We proceed with the TZ2P/KT2 level in the gas phase. Though the TZ2P is a smaller basis set than QZ4P and the effect of solvent was not included, the results of this work obtained by TZ2P/gas-phase showed similar values when QZ4P and COSMO solvent model were used. Table S1 of ESI† shows variation of values of theoretical ^{13}C NMR chemical shifts and shielding tensors between these different level of theory, however the differences between *cis* and *trans* isomers for iodine derivative are very similar in all levels of theory used in this work.

A higher value of numerical integration (equal to 8.0) was also evaluated using the same Voronoi quadrature scheme. For both integration values, the TZ2P/gas-phase calculations display results nearest the experimental values, while the largest deviations were obtained with QZ4P basis and with inclusion of the COSMO solvent model. Fig. S1 in ESI† shows the results of ^{13}C chemical shifts obtained applying numerical integration values of 6.0 and 8.0.

3.4 NBO/NLMO analyses of components of the ^{13}C NMR shielding tensor

The diamagnetic, paramagnetic and SO components of the chemical shielding tensor of the carbon atom were calculated using the SO/KT2/TZ2P level of theory (for data from other functionals, please see Tables S2–S4, ESI†).

It can be observed (Table 2) that paramagnetic (σ_{para}) and SO (σ_{SO}) components of shielding were responsible ($\sim$10 ppm each one) for the difference in the ^{13}C NMR shielding between the *cis* and *trans* isomers of iodine derivatives. For both isomers, the σ_{SO} increases from fluorine to iodine, which is more pronounced for the *trans* isomer. For the σ_{para}, more negative values are observed from chlorine to iodine for the *cis* isomer, whereas for the *trans* isomer, more positive values were found. The diamagnetic term (σ_{dia}) did not show significant changes for both isomers with the same halogen atom; thus, it cannot be used to describe the differences in the ^{13}C NMR chemical shifts of the 1,2-dihaloethenes. Thus, the paramagnetic and SO terms contribute to the lower frequency (more shielded) of the ^{13}C NMR chemical shift in the *trans* isomer.

Table 2 Theoretical (δ_{theo}[a,b]) ^{13}C NMR chemical shifts, the nuclear shielding tensor (σ_{total}[c]) and the diamagnetic (σ_{dia}), paramagnetic (σ_{para}) and spin–orbit (σ_{So}) components obtained for *cis*- and *trans*-1,2-dihaloethenes, calculated at the KT2/TZ2P level and using the SO-ZORA Hamiltonian

	cis					*trans*				
	σ_{dia}	σ_{para}	σ_{SO}	σ_{total}	δ_{theo}	σ_{dia}	σ_{para}	σ_{SO}	σ_{total}	δ_{theo}
F	240.4	−187.0	1.3	54.8	140.2	240.6	−195.5	1.2	46.3	148.6
Cl	247.8	−178.9	3.1	72.0	122.9	247.5	−178.7	3.3	72.4	122.5
Br	244.4	−179.6	12.0	76.7	118.2	244.2	−174.9	14.6	84.1	110.8
I	246.2	−181.9	25.7	90.0	104.9	246.6	−170.3	35.9	112.1	82.7

[a] $\delta_{theo} = \sigma_{TMS} - \sigma_{total}$. [b] The TMS shielding tensor is 194.9 ppm for the respective level of theory. [c] $\sigma_{total} = \sigma_{dia} + \sigma_{para} + \sigma_{SO}$.

According to Section 1 of this work, the role of the s-character of LA and the HOMO–LUMO energy gap are factors that may affect the ^{13}C shielding. Table 3 does not show significant variation in the s% of the LA. Due to the similarity between the *cis* and *trans* isomers, the s-character and certain geometric parameters, such as bond length (r_{C-X}), did not display important differences. The angle C=C–X was the only parameter that exhibited significant changes among the isomers, in particular on the *cis* isomer of iodine compounds, which is a sign of the steric repulsion between iodine atoms.

The energy gaps between occupied and virtual MOs were important in understanding certain trends in the nuclear shielding tensor, mainly because the σ_{para} and σ_{SO} consider these energies' differences in the denominator of eqn (2). The MOs energy diagram shown in Fig. 4 reveals that the profile is very similar for both isomers in the halogen series. The HOMO is a combination of the p orbitals of two carbon atoms and the p orbitals of halogen atoms with the same symmetry, which may be associated with the π orbital and $LP_3(X)$ in the localized approach, respectively. These HOMOs displayed low energy

Table 3 Geometric parameters and s-character of carbon and halogen atoms for *cis*- and *trans*-1,2-dihaloethenes calculated by applying SR-ZORA at the KT2/TZ2P level of theory

	cis					*trans*				
	r_{C-X}[a]	$r_{C=C}$[a]	$\angle_{C=C-X}$[b]	s% C	s% X	r_{C-X}[a]	$r_{C=C}$[a]	$\angle_{C=C-X}$[b]	s% C	s% X
F	1.337	1.327	122.5	24.2	25.2	1.344	1.326	119.8	23.8	24.7
Cl	1.713	1.334	124.2	24.8	17.5	1.722	1.331	121.1	24.2	17.1
Br	1.859	1.334	124.8	23.4	13.2	1.870	1.330	121.1	22.6	12.7
I	2.052	1.336	127.2	23.2	11.4	2.062	1.332	122.2	22.5	11.0

[a] In Ångströms. [b] In °.

variations, whereas the energy of the LUMOs decreased from fluorine to iodine, largely due to the stabilization of the π^* and σ_{C-X}^* antibonding orbitals.

For fluorine isomers, the largest (most negative) value of the paramagnetic component was observed for the *trans* isomer, and it was the main component responsible for the 8.5 ppm difference in the ^{13}C chemical shift (Table 1). Analyzing the HOMO–LUMO energy gap of the fluorine compounds revealed a smaller energy difference for the *trans* than for the *cis* isomer due to the higher energy of the HOMO and lower energy of the LUMO for the *trans* isomer in comparison with the *cis* isomer. This point might be a reason for the larger magnitude of the paramagnetic shielding in the *trans* isomer for difluoroethene.

The HOMO–LUMO energy gap remained smaller for the *trans* isomer from chlorine to iodine compounds; however, the σ_{para} values were almost identical for the chlorine isomers, and they were larger for the *cis* isomer in the bromine and iodine derivatives. Based on these results, the HOMO–LUMO gap is not sufficient to explain the σ_{para} values, particularly in the iodine isomers where the σ_{para} difference is larger (11.6 ppm) than the σ_{SO} variation (10.2 ppm) among *cis* and *trans* isomers. The dependence of the σ_{SO} on the HOMO–LUMO energy gap is not also clear, despite the higher stabilization of the LUMO in the *trans* isomers of the bromine and iodine compounds.

Nonetheless, Fig. 4 shows a significant destabilization of the HOMO−1 in the *cis* isomer with increasing atomic number of the halogen, whose MO has a high contribution of the p orbitals of the carbon atoms oriented in-plane of the structure. In the NBO/NLMO methodology, these orbitals are localized as $LP_2(X)$, and this behavior may be related to the steric repulsion between HA in the *cis* configuration. Most likely this increase in energy is associated with the σ_{para} and σ_{SO} trends.

As the s-character and HOMO–LUMO energy gap did not describe all the trends and values obtained, it was necessary to use other methodology to find the reasons the difference in σ_{para} and σ_{SO}. For this purpose, the σ_{para} and σ_{SO} values were analyzed in terms of each PAS coordinate (σ_{11}, σ_{22} and σ_{33}) and which NBO/NLMO orbitals would be responsible for these data.

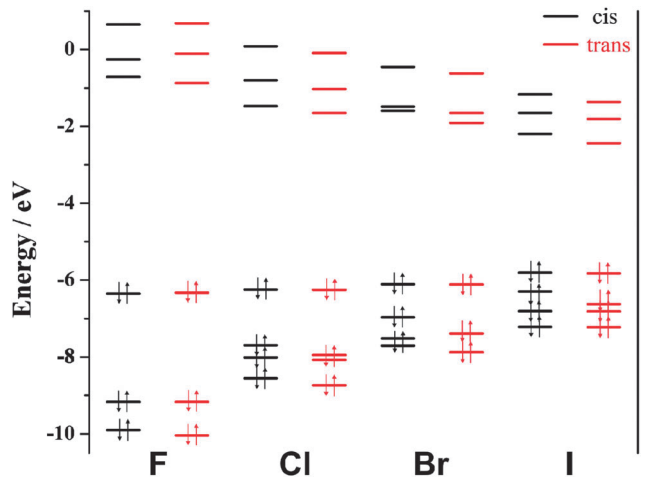

Fig. 4 Energies of frontier MOs for *cis*- and *trans*-1,2-dihaloethenes calculated at the KT2/TZ2P level.

Table 4 shows how the components of ^{13}C shielding tensor differ in the function of the PAS orientation. In general, the differences in σ_{dia} remained negligible, whereas for σ_{para} and σ_{SO}, interesting trends were observed between the *cis* and *trans* isomers and in the halogen series. Graphical representations of the ^{13}C NMR shielding tensor were built in the same way as in ref. 57 and 58.

In Fig. 5, it is possible to observe that the shielding surface is larger for *trans*-diiodoethene, and both representations show strong anisotropic character, mainly in the plane of the σ_{C-I} bond. This behavior also occurs for other halogen compounds, whose representations can be observed in Fig. S2–S4, in the ESI.†

The data in Table 4 indicate that σ_{para} differences in the fluorine isomers are dominated by the σ_{22} component of the shielding tensor. For chlorine isomers, the values do not show significant variations, and therefore the ^{13}C shielding tensors were highly similar between the two configurations. The more interesting results were obtained for the bromine and iodine compounds, where different orientations of the shielding tensor were responsible for the values of σ_{para} and σ_{SO}.

As briefly mentioned above, σ_{11} was identified as the tensor component with more influence on the σ_{para} for bromine and iodine derivatives. This orientation of the tensor always exhibited a deshielding character in the *cis* isomer for all halogens (Fig. 5 and Fig. S1–S3, from ESI†). For the *trans* isomer, deshielding character was observed for F, Cl and Br halogens, whereas for iodine, a shielding character is observed, as observed in Fig. 5. The σ_{22} component contributes to the σ_{para} and σ_{SO} components but with less extension than σ_{11} and σ_{33}.

SO coupling exhibited the largest difference between *cis* and *trans* isomers of the bromine and iodine derivatives at the σ_{33} PAS component (Table 4), suggesting that this component must be evaluated in detail to assign the origin of the SO difference between *cis* and *trans*.

Each component of the ^{13}C nuclear shielding tensor was decomposed in terms of NBOs and NLMO analysis. Fig. 6 and 7 reveal the nuclear shielding decomposition in terms of groups of NBO and NLMO with more variation; however, the complete tables containing all contributions can be observed in Tables S5 and S6, of the ESI.† NLMO analysis was chosen to describe the shielding contributions of halogen lone pairs as the contributions become small in the NBO description. This statement was determined by Mocho and Autschbach[16] in nuclear magnetic shielding in LaX_3 systems. The results shown in Fig. 6 indicate which NBO orbitals are associated with the largest magnitude of the σ_{para} component and the smallest σ_{SO} term in the *cis* isomer along the halogen series.

Stereoelectronic effects were identified as the main reasons for changes in the values of σ_{para} and σ_{SO} between *cis*- and *trans*-dihaloethene isomers based on the influence of the halogen LPs and their correlations with other orbitals. As previously revealed, the σ_{11} component is responsible for the largest variation in the σ_{para}, and this statement may be associated

Table 4 Contributions of the ^{13}C NMR shielding tensor and their diamagnetic (σ_{dia}), paramagnetic (σ_{para}) and spin–orbit (σ_{SO}) components to each PAS orientation for *cis*- and *trans*-1,2-dihaloethenes, calculated at the SO/KT2/TZ2P level

		σ_{dia}			σ_{para}			σ_{SO}			σ_{total}		
		σ_{11}	σ_{22}	σ_{33}	σ_{11}	σ_{22}	σ_{33}	σ_{11}	σ_{22}	σ_{33}	σ_{11}	σ_{22}	σ_{33}
cis	F	252.4	253.5	215.8	−276.3	−165.3	−119.3	1.2	1.0	1.7	−22.8	89.1	98.2
	Cl	258.7	260.1	224.8	−278.9	−162.9	−94.8	2.3	3.0	3.8	−18.0	100.2	133.8
	Br	257.7	257.4	218.6	−282.2	−163.9	−92.8	8.1	12.3	15.0	−16.3	105.8	140.7
	I	261.7	257.9	219.3	−289.5	−162.6	−90.6	11.1	34.3	28.3	−16.7	129.6	157.0
trans	F	253.1	252.9	216.1	−280.5	−184.5	−121.6	0.8	1.1	1.6	−26.5	69.5	96.0
	Cl	260.3	257.9	224.5	−278.9	−162.9	−94.8	2.1	6.9	1.7	−16.6	101.8	131.9
	Br	261.3	253.5	218.2	−274.6	−157.7	−92.3	7.9	15.2	20.7	−5.4	111.0	146.6
	I	266.5	253.3	220.3	−271.9	−154.3	−83.2	13.4	42.0	50.3	8.0	141.1	187.5

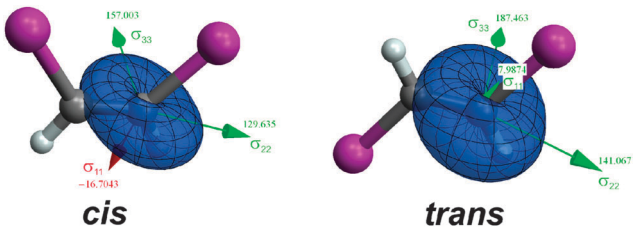

Fig. 5 Graphical representations of ^{13}C NMR shielding tensor for *cis*- and *trans*-diiodoethene. The arrows display the signs of the shielding tensor (red for negative terms and green for positive ones), and the surface indicates the magnitude of the shielding for a magnetic field in the direction of the carbon nucleus to a point on the surface *via* its distance from the carbon (polar plot).

with the decreasing trends of LP_3X_β, $\pi_{C=C}$* and σ_{C-X}* orbitals for *cis* isomers. These NBO/NLMO contributions can be rationalized by the p orbital rotation model,[57–59] mostly because the action of the angular momentum operator in the LP_3 of the halogen bonded to the neighboring carbon atom can lead to a rotation. The action of the angular momentum in the *x* axis (L_x) on the $LP_3(X_\beta)$ rotates this orbital and may provide overlap with the σ_{C-X}* orbital in the *cis* isomer (Fig. 8A), resulting in larger paramagnetic shielding because the operators OP and OZ (eqn (1)) are related to the angular momentum.

The symmetry also affects σ_{para} when $\sigma_{C\beta-H}$ for *trans* and $\sigma_{C\beta-X}$ for *cis* are compared, as in Fig. 6. These orbitals can also rotate and show symmetry with the σ_{C-X}* orbital due to the action of the angular momentum operator in the *y* axis (L_y), resulting in paramagnetic shielding (Fig. 8B). The energy of σ_{C-X} increases (see Tables S7 and S8, ESI†) with the halogen atomic number, leading to an increase in magnitude of σ_{para} for the *cis* isomer.

The steric repulsion between halogen LPs in the *cis* configuration also showed an interesting influence on σ_{para}. It is possible to observe, in Fig. 7, that LP_2X_β causes strong paramagnetic shielding in bromine and iodine compounds of *cis* isomers, whereas no significant changes in the *trans* isomers are observed.

The effects of steric interactions between LP_2 orbitals was easier to envision on the SO shielding at the σ_{33} component,

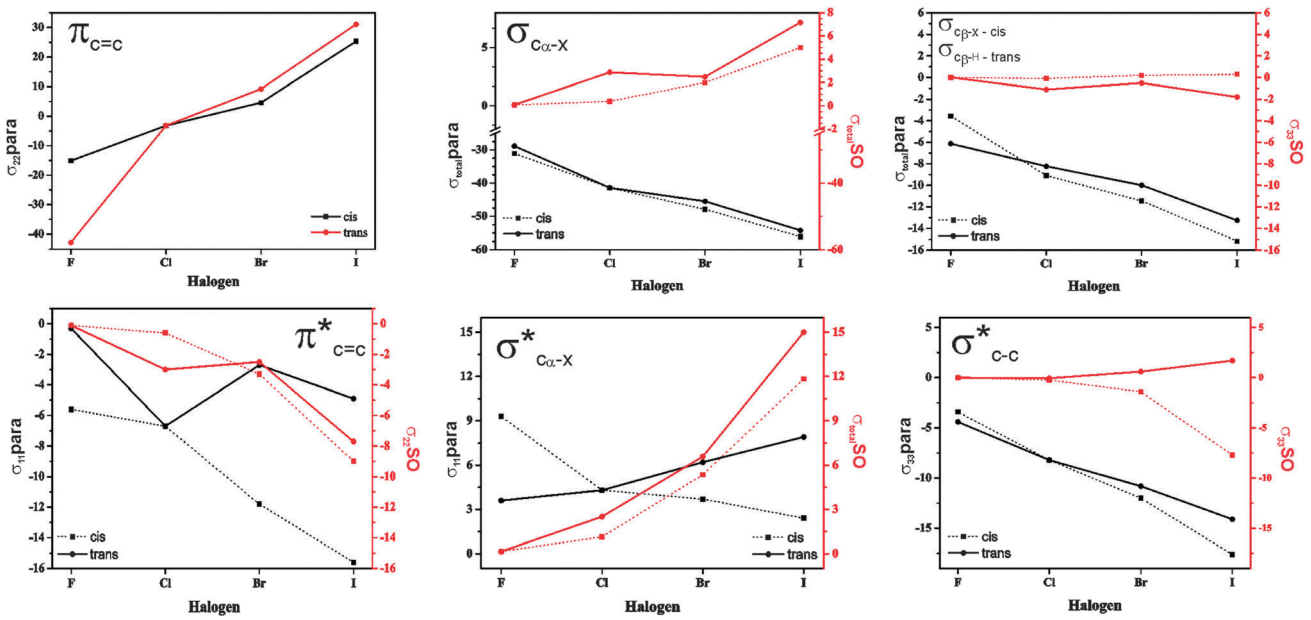

Fig. 6 NBO contributions (in ppm) for the paramagnetic and spin–orbit components of the ^{13}C NMR shielding tensor for the PAS coordinate with more significant variation between *cis* and *trans* isomers and in the halogen series. The data were obtained by the SO/KT2/TZ2P level.

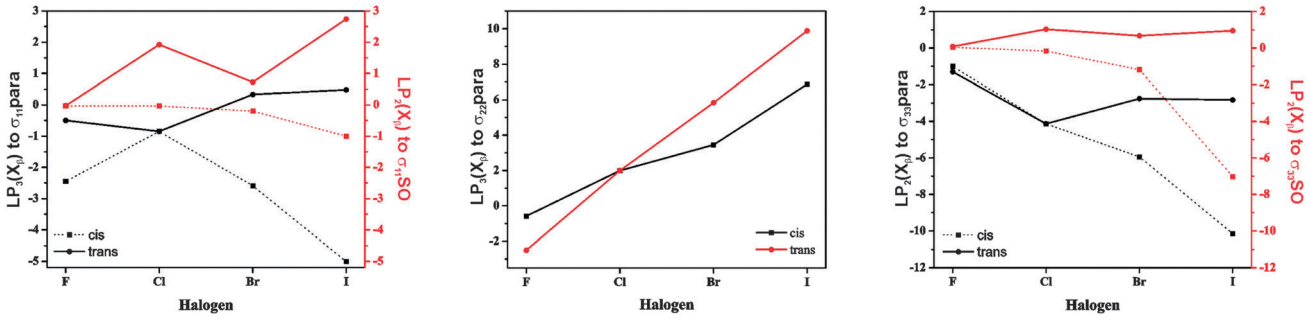

Fig. 7 NLMO contributions (in ppm) of the halogen *lone pairs* (LP) for the paramagnetic and spin–orbit components of the ^{13}C NMR shielding tensor for the PAS coordinate with more significant variation between *cis* and *trans* isomers and in the halogen series. The data were obtained by the SO/KT2/TZ2P level. X_β is bonded to a carbon atom neighboring the calculated ^{13}C.

whose PAS orientation was responsible for the largest variation in σ_{SO}. The plot for LP_2 (Fig. 7) suggests that steric repulsion between iodine LP_2 occurs and may be the reason for the lower ^{13}C NMR shielding tensor of the *cis*-diiodoethene. The LP_2X_β did not affect the SO coupling of *trans*-diiodoethene (σ_{SO} = 0.95 ppm), but the deshielding was very strong in *cis*-diiodoethene (σ_{SO} = −7.02 ppm) due to the steric repulsion. The effect of steric compression is more pronounced at the σ_{33} component as a result of rotation of LP_2(I).

A relationship between steric hindrance and hyperconjugative interactions has been suggested, although dissenting opinions remain.[62,63] In any case, our results indicate that such effects may explain the higher frequency of ^{13}C NMR of the *cis* isomer for bromine and iodine derivatives. It has been discussed in the literature[62] that NBOs may lead to different interpretations from orbitals obtained by other localization procedures.[63] The NBO shielding analysis was indeed unable to identify the steric repulsion between iodine atoms, though this behavior is not surprising.[16,62] However, the NLMOs are similar to orbitals obtained with other localization techniques and appear as a suitable option for determining the contributions of LPs.[16] In this study the delocalization interactions were essential in supporting the role of antibonding orbitals and relating them to the orbital rotation model and the paramagnetic shielding.

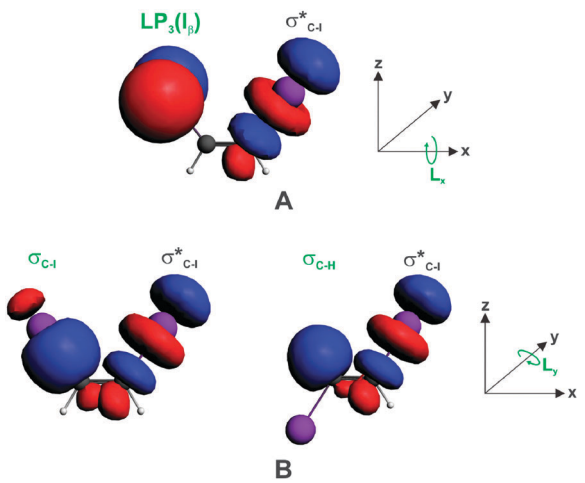

Fig. 8 Representation of occupied NBOs that may rotate and show overlap with the σ_{C-I}* orbital due to the action of the angular momentum operators L_x (A) and L_y (B).

3.5 Dependency of the steric effects on the angle C═C–I for *cis* isomer

To verify our hypothesis about the influence of steric interaction on the HALA effect, the C═C–I bond angle was changed from 90° to 140° in 10° steps (Fig. 9), and the shielding tensor was calculated for each molecular arrangement. It is known that the SO term depends heavily on the bond and dihedral angles in the molecule.[25] In this study, the C═C–I bond angle was changed to gauge variation in the nuclear shielding tensor between the *cis* and *trans* isomers. The main difference between the two isomers when the bond angles C═C–I were changed from 90° to 140° was relief of the steric interaction between two iodine atoms in the *cis* isomer, suggesting that steric interaction affects the nuclear shielding tensor.

For the *trans* isomer, the shielding tensors do not change significantly in comparison with the *cis* isomer due to the relief of steric repulsion between the iodine atoms. In the *cis* isomer, the ^{13}C shielding tensor was strongly affected by the angle C═C–I, whose magnitude of shielding reached similar values as for *trans* at the bond angle equal to 140°. This behavior may be observed through the analysis of the HOMO–LUMO energy gap, which can be observed in Fig. S5 in the ESI.† The energy results of HOMO and HOMO−1 of the *cis* isomer showed a similar profile to the *trans* isomer when the C═C–I angle was equal to 140°. The energy of HOMO−1 increased significantly with proximity of the iodine atoms, in other words with increasing steric interaction.

NBO analysis of the *cis* geometry with the angle C═C–I equal to 140° suggested a decrease in the deshielding caused by the LP_2X_β for both σ_{para} and σ_{SO} components. Unlike the equilibrium geometry, at the angle of 140°, the σ_{11} component displayed positive shielding, as observed in Fig. 10. The SO shielding on σ_{33} increased with increasing bond angle, whose effect of LP_2X_β decreased from −7.02 ppm (equilibrium geometry) to −2.22 ppm (bond angle equal to 140°), resulting in the ^{13}C NMR shielding more nearest of the *trans* isomer. However, this SO shielding was smaller than the total changes. The reason for the shielding increase for the structure with the

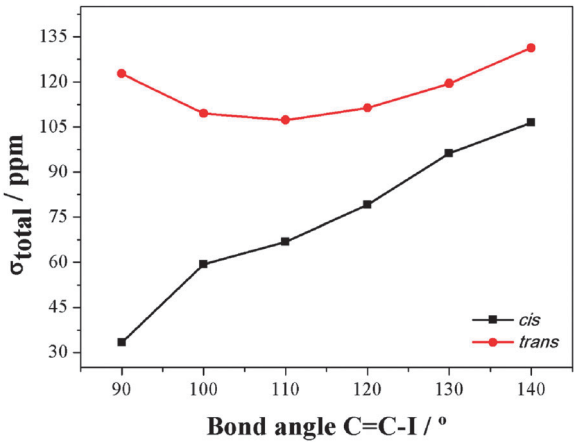

Fig. 9 The theoretical magnetic nuclear shielding tensor of carbon atoms (σ_{total}) for *cis*- and *trans*-1,2-diiodoethene, varying the C=C–I bond angle from 90° to 140° in 10° steps. The data were calculated with the KT2/TZ2P functional, using the SO-ZORA Hamiltonian.

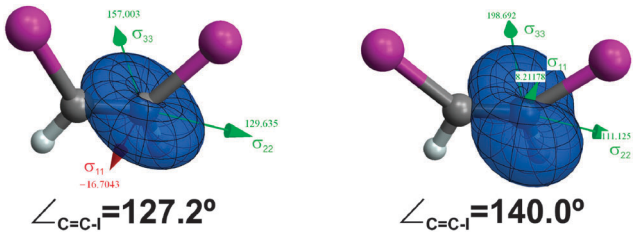

Fig. 10 Graphical representations of ^{13}C NMR shielding tensor for *cis*-diiodoethene at the equilibrium angle (127.2°) and 140°. The arrows display the signs of the shielding tensor (red for negative terms and green for positive ones), and the surface indicates the magnitude of the shielding for a magnetic field in the direction of the carbon nucleus to a point on the surface *via* its distance from the carbon (polar plot).

bond angle equal to 140° may be the s-character at the carbon atom as a significant increase of s-character from 21.5% to 27.3% was observed with increasing bond angle (95° to 140°).

These results corroborate that for the studied systems, the steric and hyperconjugative interactions play important roles in explaining the experimental behavior for the ^{13}C NMR chemical shift *via* the involvement of certain LPs in the paramagnetic and SO component of the ^{13}C shielding tensor.

4. Conclusions

The results described in this study indicate that the electronic structure has a large influence on the HALA effect, which is known to decrease the ^{13}C NMR chemical shift in cases such as the normal halogen dependence. In very similar systems, namely the case of the *cis*- and *trans*-1,2-dihaloethenes isomers, a considerable change was observed in the spin–orbit and the paramagnetic components for the total shielding tensor in the ^{13}C NMR chemical shift. The differences in the magnetic shielding tensors between the isomers of 1,2-dihaloethenes (halo = F, Cl, Br or I) were explained in terms of the HOMO–LUMO energy gap, rotation model and stereoelectronic interactions, and it has been described how the SO/FC transmission mechanism could be affected by these effects.

The principal factor responsible for the difference (17 ppm) in the ^{13}C NMR chemical shift between the *cis*- and *trans*-diiodoethene isomers was the steric interaction observed between the two iodine atoms in the *cis* isomer, which provided different values for SO and paramagnetic shielding. The effect of steric interactions on the magnitude of the ^{13}C shielding tensor was evaluated in terms of the contributions of the NBO/NLMO orbitals to the ^{13}C shielding for each PAS coordinate, allowing a better description of the theoretically observed variations associated with experimental data. This study highlights how similar systems, such as *cis–trans* configuration, can lead to considerable differences in NMR parameters.

Acknowledgements

We are grateful to FAPESP for the financial support (2011/17357-3 and 2013/03477-2), a scholarship to R.V.V. (2012/12414-1) and a fellowship to L.C.D. (2010/15765-4 and 2014/21930-9) and to CNPq for a fellowship to C.F.T. J.A. acknowledges financial support from the National Science Foundation (CHE-1265833).

References

1 J. Autschbach, in *High Resolution NMR Spectroscopy: Understanding Molecules and Their Electronic Structures*, ed. R. H. Contreras, Elsevier, Oxford, 2013, ch. 4, pp. 69–112.
2 J. Autschbach and T. Ziegler, in *Encyclopedia of Nuclear Magnetic Resonance*, ed. D. M. Grant and R. K. Harris, Wiley-VCH, Chichester, 2002, vol. 9.
3 P. Pyykkö, *Chem. Rev.*, 1988, **88**, 563–594.
4 T. Yoshizawa and S. Sakaki, *J. Comput. Chem.*, 2013, **34**, 1013–1023.
5 P. Pyykkö, *Annu. Rev. Phys. Chem.*, 2012, **63**, 45–64.
6 M. Reiher and A. Wolf, *Relativistic Quantum Chemistry: The Fundamental Theory of Molecular Science*, Wiley-VCH, Weinheim, 2009.
7 S. Zheng and J. Autschbach, *Chem. – Eur. J.*, 2011, **17**, 161–173.
8 J. Autschbach, K. Sutter, L. A. Truflandier, E. Brendler and J. Wagler, *Chem. – Eur. J.*, 2012, **18**, 12803–12813.
9 J. Vícha, M. Patzschke and R. Marek, *Phys. Chem. Chem. Phys.*, 2013, **15**, 7740–7754.
10 P. Hrobárik, V. Hrobáriková, F. Meier, M. Repiský, S. Komorovský and M. Kaupp, *J. Phys. Chem. A*, 2011, **115**, 5654–5659.
11 K. Bouzková, M. Babinský, L. Novosadová and R. Marek, *J. Chem. Theory Comput.*, 2013, **9**, 2629–2638.
12 A. Gryff-Keller, A. Kraska-Dziadecka, S. Molchanov and A. Wodyński, *J. Phys. Chem. A*, 2012, **116**, 10615–10620.
13 M. Babinský, K. Bouzková, M. Pipíska, L. Novosadová and R. Marek, *J. Phys. Chem. A*, 2013, **117**, 497–503.

14 V. G. Malkin, O. L. Malkina and D. R. Salahub, *Chem. Phys. Lett.*, 1996, **261**, 335–345.
15 J. Vaara, O. L. Malkina, H. Stoll, V. G. Malkin and M. Kaupp, *J. Chem. Phys.*, 2001, **114**, 61–71.
16 S. Moncho and J. Autschbach, *Magn. Reson. Chem.*, 2010, **48**, S76–S85.
17 M. W. Lodewyk, M. R. Siebert and D. J. Tantillo, *Chem. Rev.*, 2012, **112**, 1839–1862.
18 P. Lantto, J. Vaara, A. M. Kantola, V. Telkki, B. Schimmelpfennig, K. Ruud and J. Jokisaari, *J. Am. Chem. Soc.*, 2002, **124**, 2762–2771.
19 P. Lantto, R. H. Romero, S. S. Gómez, G. A. Aucar and J. Vaara, *J. Chem. Phys.*, 2006, **125**, 184113.
20 M. Kaupp, in *Relativistic Electronic Structure Theory, Part 2: Applications*, ed. P. Schwerdtfeger, Elsevier, Oxford, 2004, ch. 9, vol. 2, pp. 552–597.
21 J. Autschbach and S. Zheng, *Annu. Rep. NMR Spectrosc.*, 2009, **67**, 1–95.
22 R. G. Kidd, *Annu. Rep. NMR Spectrosc.*, 1980, **10A**, 1–79.
23 V. Barone, R. H. Contreras, E. Díez and A. Esteban, *Mol. Phys.*, 2003, **101**, 1297–1301.
24 A. A. Cheremisin and P. V. Schastnev, *J. Magn. Reson.*, 1980, **40**, 459–468.
25 M. Kaupp, O. L. Malkina, V. G. Malkin and P. Pyykkö, *Chem. – Eur. J.*, 1998, **4**, 118–126.
26 M. Hyvärinen, J. Vaara, A. Goldammer, B. Kutzky, K. Hegetschweiler, M. Kaupp and M. Straka, *J. Am. Chem. Soc.*, 2009, **131**, 11909–11918.
27 S. K. Wolff and T. Ziegler, *J. Chem. Phys.*, 1998, **109**, 895–905.
28 K. Hegetschweiler, D. Kuppert, J. Huppert, M. Straka and M. Kaupp, *J. Am. Chem. Soc.*, 2004, **126**, 6728–6738.
29 A. Cunha Neto, L. C. Ducati, R. Rittner, C. F. Tormena, R. H. Contreras and G. Frenking, *J. Chem. Theory Comput.*, 2009, **5**, 2222–2228.
30 J. Vícha, M. Straka, M. L. Munzarová and R. Marek, *J. Chem. Theory Comput.*, 2014, **10**, 1489–1499.
31 J. Autschbach, *Mol. Phys.*, 2013, **111**, 2544–2554.
32 L. J. Mueller, *Concepts Magn. Reson.*, 2011, **38A**, 221–235.
33 R. R. Ernst, G. Bodenhausen and A. Wokaun, *Principles of Nuclear Magnetic Resonance in One and Two Dimensions*, Oxford, New York, 1987.
34 G. T. Velde, F. M. Bickelhaupt, E. J. Baerends, C. F. Guerra, S. J. A. van Gisbergen, J. G. Snijders and T. Ziegler, *J. Comput. Chem.*, 2001, **22**, 931–967.
35 T. Saue, *ChemPhysChem*, 2011, **12**, 3077–3094.
36 J. Autschbach, *J. Chem. Phys.*, 2012, **136**, 150902.
37 S. K. Wolff, T. Ziegler, E. van Lenthe and E. J. Baerends, *J. Chem. Phys.*, 1999, **110**, 7689–7698.
38 E. van Lenthe, J. G. Snijders and E. J. Baerends, *J. Chem. Phys.*, 1996, **105**, 6505–6513.
39 Y. Xiao, Q. Sun and W. Liu, *Theor. Chem. Acc.*, 2012, **131**, 1080.
40 J. Autschbach and T. Ziegler, *Coord. Chem. Rev.*, 2003, **238–239**, 83–126.
41 J. Autschbach and S. Zheng, *Magn. Reson. Chem.*, 2008, **46**, S45–S55.
42 J. Schraml, *Collect. Czech. Chem. Commun.*, 1976, **41**, 3063–3076.
43 G. Savitsky and K. Namikawa, *J. Phys. Chem.*, 1963, **67**, 2754–2756.
44 G. E. Maciel, P. D. Ellis, J. J. Natterstad and G. B. Savitsky, *J. Magn. Reson.*, 1969, **1**, 589–605.
45 R. M. Noyes, R. G. Dickinson and V. Schomaker, *J. Am. Chem. Soc.*, 1945, **67**, 1319–1329.
46 R. Ditchfield and P. D. Ellis, *Chem. Phys. Lett.*, 1972, **17**, 342–344.
47 A. D. Becke, *J. Chem. Phys.*, 1993, **98**, 5648–5652.
48 J. P. Perdew, *Phys. Rev. B: Condens. Matter Mater. Phys.*, 1986, **33**, 8822–8824.
49 T. W. Keal and D. J. Tozer, *J. Chem. Phys.*, 2003, **119**, 3015–3024.
50 C. Adamo and V. Barone, *J. Chem. Phys.*, 1999, **110**, 6158–6170.
51 E. J. Baerends, T. Ziegler, J. Autschbach, D. Bashford, A. Bérces, F. M. Bickelhaupt, C. Bo, P. M. Boerrigter, L. Cavallo, D. P. Chong, L. Deng, R. M. Dickson, D. E. Ellis, M. van Faassen, L. Fan, T. H. Fischer, C. Fonseca Guerra, M. Franchini, A. Ghysels, A. Giammona, S. J. A. van Gisbergen, A. W. Götz, J. A. Groeneveld, O. V. Gritsenko, M. Grüning, S. Gusarov, F. E. Harris, P. van den Hoek, C. R. Jacob, H. Jacobsen, L. Jensen, J. W. Kaminski, G. van Kessel, F. Kootstra, A. Kovalenko, M. V. Krykunov, E. van Lenthe, D. A. McCormack, A. Michalak, M. Mitoraj, S. M. Morton, J. Neugebauer, V. P. Nicu, L. Noodleman, V. P. Osinga, S. Patchkovskii, M. Pavanello, P. H. T. Philipsen, D. Post, C. C. Pye, W. Ravenek, J. I. Rodríguez, P. Ros, P. R. T. Schipper, G. Schreckenbach, J. S. Seldenthuis, M. Seth, J. G. Snijders, M. Solà, M. Swart, D. Swerhone, G. te Velde, P. Vernooijs, L. Versluis, L. Visscher, O. Visser, F. Wang, T. A. Wesolowski, E. M. van Wezenbeek, G. Wiesenekker, S. K. Wolff, T. K. Woo and A. L. Yakovlev, *ADF2013, SCM, Theoretical Chemistry*, Vrije Universiteit, Amsterdam, The Netherlands, 2013, http://www.scm.com.
52 E. van Lenthe, A. Ehlers and E. J. Baerends, *J. Chem. Phys.*, 1999, **110**, 8943–8953.
53 E. van Lenthe, E. J. Baerends and J. G. Snijders, *J. Chem. Phys.*, 1993, **99**, 4597–4610.
54 A. Klamt and G. Schüürmann, *J. Chem. Soc., Perkin Trans. 2*, 1993, 799–805.
55 C. C. Pye and T. Ziegler, *Theor. Chem. Acc.*, 1999, **101**, 396–408.
56 E. D. Glendening, J. K. Badenhoop, A. E. Reed, J. E. Carpenter, J. A. Bohmann, C. M. Morales, C. R. Landis and F. Weinhold, *NBO 6.0*, Theoretical Chemistry Institute, University of Wisconsin, Madison, 2013.
57 E. Zurek, C. Pickard and J. Autschbach, *J. Phys. Chem. A*, 2009, **113**, 4117–4124.
58 J. Autschbach, S. Zheng and R. W. Schurko, *Concepts Magn. Reson., Part A*, 2010, **36**, 84–126.
59 J. Autschbach, *J. Chem. Phys.*, 2008, **128**, 1641112.
60 K. B. Wiberg, J. D. Hammer, K. W. Zilm and J. R. Cheeseman, *J. Org. Chem.*, 1999, **64**, 6394–6400.
61 J. B. Grutzner, *Recent advances in organic NMR spectroscopy*, NRl Press Landisviller, New Jersey, 1987.
62 F. M. Bickelhaupt and E. J. Baerends, *Angew. Chem., Int. Ed.*, 2003, **42**, 4183–4188.
63 F. Weinhold, *Angew. Chem., Int. Ed.*, 2003, **42**, 4188–4194.

